NUMERICAL SIMULATION OF SUPERSONIC AXISYMMETRIC FLOW OVER MISSILE AFTERBODY WITH JET EXHAUST USING POSITIVE SCHEMES

Zhu Sunke[1], *Ma Dawei*[1], *Chen Eryun*[2], *Le Guigao*[1]

(1. School of Mechanical Engineering, Nanjing University of Science and Technology, Nanjing, 210094, P. R. China;
2. School of Energy and Power Engineering, Shanghai University of Science and Technology, Shanghai, 200093, P. R. China)

Abstract: Supersonic axisymmetric jet flow over a missile afterbody containing exhaust jet is simulated using the second order accurate positive schemes method developed for solving the axisymmetric Euler equations based on the 2-D conservation laws. Comparisons between the numerical results and the experimental measurements show excellent agreements. The computed results are in good agreement with the numerical solutions obtained by using third order accurate RKDG finite element method. The results show larger gradient at discontinuous points compared with those obtained by second order accurate TVD schemes. It indicates that the presented method is efficient and reliable for solving the axisymmetric jet with external freestream flows, and shows that the method captures shocks well without numerical noise.

Key words: computational fluid dynamics; supersonic flow; positive schemes; numerical simulation

CLC number: V211.3 **Document code**: A **Article ID**: 1005-1120(2011)03-0255-07

INTRODUCTION

During supersonic flight, the intensely interactions between the exhaust jet and the external supersonic freestream flows in the afterbody flow fields are extremely complex, which can seriously affect the travel features, cause stability problem and impact control effectiveness of the jet-propelled missile or rocket. Experimental studies[1-4] of such flow have been extensively carried out in the past several decades. However, the detailed experiment is not only complex and expensive, but also not enough to understand the complex physics in many cases.

Numerical simulation is an effective method to obtain valuable insights into the flow-field structures, which is easy and inexpensive as well as can provide much more details. Le et al[5] used the total variation diminishing (TVD) scheme to solve the mixture flow Euler equations for the supersonic underexpanded jet exhausting from a rocket nozzle and the external supersonic flow. Chen et al[6] investigated supersonic inviscid flows in missile propulsive jet with discontinuous finite element method. Sahu et al[7-8] simulated the supersonic flow over a missile afterbody containing a centered exhaust jet employing the beam-warming finite difference scheme.

At the middle of 1990s, Liu and Lax[9-10] introduced the positive scheme finite difference method for solving hyperbolic systems of conservation laws, which is second order accurate both in the space and the time and has a very simple structure. A lot of numerical results showed that the positive schemes were competitive with other high order accurate schemes.

Foundation items: Supported by the National Natural Defense Basic Scientific Research Program of China (A262006-1288); the Key Disciplines Program of Shanghai Municipal Commission of Education (J50501).

Received date: 2010-06-21; **revision received date**: 2011-03-31

E-mail: suncobest@163.com

In this paper, the positive scheme method with second accuracy, which is extended for solving the axisymmetric Euler equations based on Refs. [9,10], is used to numerically simulate the flow fields resulting from the supersonic axisymmetric jet flow over a missile afterbody with jet exhaust. In general, all the essential flow features of the numerical solutions are in good agreement with those of experiment and other numerical schemes, which demonstrates that the development for positive schemes is successful and the presented method is robust. It provides a new means for numerical study of the jet flow fields.

1 MATHEMATICAL MODEL

1.1 Governing equations

For supersonic jet flow, the governing equations can be expressed as the inviscid, axisymmetric Euler equations in the cylindrical coordinate system[5,6,11]

$$\frac{\partial \boldsymbol{U}}{\partial t}+\frac{\partial \boldsymbol{F}(\boldsymbol{U})}{\partial x}+\frac{\partial \boldsymbol{G}(\boldsymbol{U})}{\partial y}=\boldsymbol{S}(\boldsymbol{U}),\Omega\times(0,T) \tag{1}$$

where $\boldsymbol{U}=[\rho,\rho u,\rho v,E]^{\mathrm{T}}$, $\boldsymbol{F}(\boldsymbol{U})=[\rho u,\rho u^2+p,\rho uv,(E+p)u]^{\mathrm{T}}$, $\boldsymbol{G}(\boldsymbol{U})=[\rho v,\rho uv,\rho v^2+p,(E+p)\cdot v]^{\mathrm{T}}$, $\boldsymbol{S}(\boldsymbol{U})=(-\rho v/y)[1,u,v,(E+p)/\rho]^{\mathrm{T}}$, $\Omega\in\mathbf{R}^2$. u and v are the velocity components along the x and y directions, respectively. T is the time, ρ the density, p the pressure, and E the total energy per unit volume. The total energy is the sum of the internal energy and the kinetic energy

$$E=\rho e+\rho(u^2+v^2)/2 \tag{2}$$

where e is the internal energy per unit mass. The pressure is given by the equation of state for perfect gas

$$p=(\gamma-1)\rho e \tag{3}$$

where γ is the ratio of specific heats.

1.2 Space discretization

The finite difference equations of the axisymmetric governing Eq. (1) discretized using the positive schemes are given in semi-discrete form as

$$\left(\frac{\partial \boldsymbol{U}}{\partial t}\right)_{i,j}=-\begin{bmatrix}\frac{1}{\Delta x}(\boldsymbol{F}_{i+1/2,j}-\boldsymbol{F}_{i-1/2,j})+\\ \frac{1}{\Delta y}(\boldsymbol{G}_{i,j+1/2}-\boldsymbol{G}_{i,j-1/2})\end{bmatrix}+\boldsymbol{S}_{i,j} \tag{4}$$

where Δx and Δy are spatial step in the x and y axes, respectively. The construction process of positive scheme numerical flux, taking $\boldsymbol{F}_{i+1/2,j}$ for example, can be described as follows briefly. Other details of the calculation technique can be found in Refs. [9-10].

The numerical flux $\boldsymbol{F}_{i+1/2,j}$ in Eq. (4) is constructed by mixing a centered difference flux $\boldsymbol{F}^{\mathrm{c}}_{i+1/2,j}$ and a upwind flux $\boldsymbol{F}^{\mathrm{up}}_{i+1/2,j}$. Introducing the limiter $\boldsymbol{L}^0=\boldsymbol{R}\mathrm{diag}(\phi^0(\theta^k))\boldsymbol{R}^{-1}$, where $\phi^0(\theta)$[12]: $0\leqslant\phi^0(\theta),\frac{\phi^0(\theta)}{\theta}\leqslant 2$ and $\phi^0(1)=1$. The numerical flux can be constructed as

$$\boldsymbol{F}^0_{i+1/2,j}=\boldsymbol{F}^{0,\mathrm{up}}_{i+1/2,j}+\boldsymbol{L}^0(\boldsymbol{F}^{0,c}_{i+1/2,j}-\boldsymbol{F}^{0,\mathrm{up}}_{i+1/2,j}) \tag{5}$$

where $\boldsymbol{F}^{0,\mathrm{c}}_{i+1/2,j}=\frac{1}{2}[\boldsymbol{F}(\boldsymbol{U}_{i,j})+\boldsymbol{F}(\boldsymbol{U}_{i+1,j})]$, $\boldsymbol{F}^{0,\mathrm{up}}_{i+1/2,j}=\frac{1}{2}[\boldsymbol{F}(\boldsymbol{U}_{i,j})+\boldsymbol{F}(\boldsymbol{U}_{i+1,j})]-\frac{1}{2}|\overset{\circ}{\boldsymbol{A}}|(\boldsymbol{U}_{i+1,j}-\boldsymbol{U}_{i,j})$, $|\overset{\circ}{\boldsymbol{A}}|=\boldsymbol{R}|\boldsymbol{\Lambda}|\boldsymbol{R}^{-1}$ is the absolute value of $\boldsymbol{A}$, $\boldsymbol{A}=\partial\boldsymbol{F}(\boldsymbol{U})/\partial\boldsymbol{U}$ and $|\boldsymbol{\Lambda}|=\mathrm{diag}(|\lambda^k|)$. Then numerical flux of the least dissipative scheme is given by

$$\boldsymbol{F}^0_{i+1/2,j}=\frac{1}{2}[\boldsymbol{F}(\boldsymbol{U}_{i,j})+\boldsymbol{F}(\boldsymbol{U}_{i+1,j})]-\frac{1}{2}|\overset{\circ}{\boldsymbol{A}}|(\boldsymbol{U}_{i+1,j}-\boldsymbol{U}_{i,j})+\frac{1}{2}\boldsymbol{L}^0|\overset{\circ}{\boldsymbol{A}}|(\boldsymbol{U}_{i+1,j}-\boldsymbol{U}_{i,j}) \tag{6}$$

If the absolute value of $\boldsymbol{A}$, $|\dot{\boldsymbol{A}}|=\boldsymbol{R}\mathrm{diag}(\mu^k)\boldsymbol{R}^{-1}$, where the diagonal matrix $\mathrm{diag}(\mu^k)\geqslant|\boldsymbol{\Lambda}|$, then with the aid of the limiter $\boldsymbol{L}^1=\boldsymbol{R}\cdot\mathrm{diag}(\phi^1(\theta^k))\boldsymbol{R}^{-1}$, where $\phi^1(\theta)=\begin{cases}0,\theta\leqslant 0\\ \theta,0<\theta\leqslant 1\\ 1,\theta>1\end{cases}$ is the minmod limiter function[13], the numerical flux can be constructed as

$$\boldsymbol{F}^1_{i+1/2,j}=\boldsymbol{F}^{1,\mathrm{up}}_{i+1/2,j}+\boldsymbol{L}^1(\boldsymbol{F}^{1,\mathrm{c}}_{i+1/2,j}-\boldsymbol{F}^{1,\mathrm{up}}_{i+1/2,j}) \tag{7}$$

where $\boldsymbol{F}^{1,\mathrm{c}}_{i+1/2,j}=\frac{1}{2}[\boldsymbol{F}(\boldsymbol{U}_{i,j})+\boldsymbol{F}(\boldsymbol{U}_{i+1,j})]$, $\boldsymbol{F}^{1,\mathrm{up}}_{i+1/2,j}=\frac{1}{2}[\boldsymbol{F}(\boldsymbol{U}_{i,j})+\boldsymbol{F}(\boldsymbol{U}_{i+1,j})]-\frac{1}{2}|\dot{\boldsymbol{A}}|(\boldsymbol{U}_{i+1,j}-\boldsymbol{U}_{i,j})$.

Similarly, numerical flux of the more dissipative scheme is expressed as

$$\boldsymbol{F}^{1}_{i+1/2,j}=\frac{1}{2}[\boldsymbol{F}(\boldsymbol{U}_{i,j})+\boldsymbol{F}(\boldsymbol{U}_{i+1,j})]-\frac{1}{2}|\dot{\boldsymbol{A}}|(\boldsymbol{U}_{i+1,j}-\boldsymbol{U}_{i,j})+\frac{1}{2}\boldsymbol{L}^{1}|\dot{\boldsymbol{A}}|(\boldsymbol{U}_{i+1,j}-\boldsymbol{U}_{i,j}) \tag{8}$$

Finally, combining the least dissipative scheme Eq. (6) and more dissipative scheme Eq. (8), the numerical flux of positive schemes can be written as

$$\boldsymbol{F}^{\alpha,\beta}_{i+1/2,j}=\frac{1}{2}[\boldsymbol{F}(\boldsymbol{U}_{i,j})+\boldsymbol{F}(\boldsymbol{U}_{i+1,j})]-\frac{1}{2}[\alpha|\overset{o}{\boldsymbol{A}}|(\boldsymbol{I}-\boldsymbol{L}^{0})+\beta|\dot{\boldsymbol{A}}|(\boldsymbol{I}-\boldsymbol{L}^{1})](\boldsymbol{U}_{i+1,j}-\boldsymbol{U}_{i,j}) \tag{9}$$

under the following CFL condition: $\frac{\Delta t}{\Delta x}(\alpha\cdot\max\limits_{1\leqslant k\leqslant n,U}|\lambda^{k}|+\beta\max\limits_{1\leqslant k\leqslant n,U}\mu^{k})\leqslant\frac{1}{2}$, where Δt is the time step. The constants α and β satisfy: $0\leqslant\alpha\leqslant1$ and $\alpha+\beta\geqslant1$.

1.3 Runge-Kutta time discretization

To match accuracy with the space variables, we construct the time discretization with second order accurate Runge-Kutta method[14-15]

$$\boldsymbol{U}^{*}_{i,j}=\boldsymbol{U}^{m}_{i,j}-\left[\frac{\Delta t}{\Delta x}(\boldsymbol{F}^{\alpha_x,\beta_x}_{i+1/2,j}-\boldsymbol{F}^{\alpha_x,\beta_x}_{i-1/2,j})+\frac{\Delta t}{\Delta y}(\boldsymbol{G}^{\alpha_y,\beta_y}_{i,j+1/2}-\boldsymbol{G}^{\alpha_y,\beta_y}_{i,j-1/2})\right]+\Delta t\boldsymbol{S}_{i,j} \tag{10a}$$

$$\boldsymbol{U}^{**}_{i,j}=\boldsymbol{U}^{*}_{i,j}-\left[\frac{\Delta t}{\Delta x}(\boldsymbol{F}^{\alpha_x,\beta_x\,*}_{i+1/2,j}-\boldsymbol{F}^{\alpha_x,\beta_x\,*}_{i-1/2,j})+\frac{\Delta t}{\Delta y}(\boldsymbol{G}^{\alpha_y,\beta_y\,*}_{i,j+1/2}-\boldsymbol{G}^{\alpha_y,\beta_y\,*}_{i,j-1/2})\right]+\Delta t\boldsymbol{S}^{*}_{i,j} \tag{10b}$$

$$\boldsymbol{U}^{m+1}_{i,j}=\frac{1}{2}\boldsymbol{U}^{m}_{i,j}+\frac{1}{2}\boldsymbol{U}^{**}_{i,j} \tag{10c}$$

2 NUMERICAL EXPERIMENTS

Fig. 1 shows the schematic diagram of computational domain for half of the axisymmetric plane of the flow field, which is 1.5 in the radial direction and 3.5 in the axial direction. The computational domain is discretized with the uniform mesh size of $\Delta x=\Delta y=1/40$. On the inflow boundary GH, the primitive variables summarized in Table 1 are specified for the calculation, where the subscript j denotes the nozzle exit value and ∞ the supersonic freestream value, Ma_∞ the Mach number of supersonic freestream, Ma_j the Mach number at the jet exit, p_j/p_∞ the ratio of nozzle exit gas stagnation pressure to ambient gas static pressure, T_j/T_∞ the ratio of nozzle exit gas stagnation temperature to ambient gas stagnation temperature. r_j and R_j are the inner and outer nozzle radius respectively. At the solid walls of nozzle EF and FG, the reflecting boundary conditions are imposed. On the upstream boundary DE the supersonic freestream condition is applied. On the outer boundary CD, simple wave condition is used. On the jet axis AB, the symmetric boundary condition is applied. On the downstream boundary BC, a simple extrapolation is imposed. The rest of the whole computational domain is initially assumed to be supersonic freestream conditions.

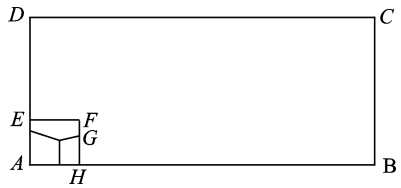

Fig. 1 Computational domain

Table 1 Test conditions

Case	Ma_∞	Ma_j	p_j/p_∞	T_j/T_∞	r_j	R_j
1	2.01	2.5	1.0	1.0	0.3	0.5
2	2.01	2.5	6.0	1.0	0.3	0.5
3	2.01	2.5	6.0	3.0	0.3	0.5

Fig. 2 shows the property contours of supersonic flow including the density and pressure corresponding to Case 1. As shown in Fig. 2, the exhaust jet is compressed by the supersonic freestream around the lip of the nozzle exit, also the Mach disc structure almost disappears near the jet upstream. Meanwhile, two oblique shock waves, contact discontinuity jet shock wave and bottle shock wave are formed. Behind the first oblique shock wave are the expansion waves around the lip of the nozzle exit and under the second oblique shock wave is jet shock wave. These expansion waves propagate across the jet

flow and are reflected back into the jet as compression waves from the jet boundary, and then an incident shock formed. Later a reflected shock wave appears when the incident shock encounters the jet centerline and intersects with jet shock wave. Overall, agreements of several primary flow characteristics between the numerical results and the experimental shadowgraph[1] obtained under the same flow condition, as shown in Fig. 2 (c), are reasonably well. It indicates that the numerical results obtained by positive schemes are reliable.

Fig. 3 shows the property contours of supersonic flow including the density and pressure corresponding to Case 2. In Fig. 3, a lambda shock wave appears which is composed of the oblique shock wave and the jet shock wave, due to the interactions between the supersonic freestream and the exhaust underexpanded jet. Between the oblique shock and jet shock, a contact discontinuity exists. The underexpanded jet is compressed by the supersonic freestream around the lip of the nozzle exit, and a reflected shock wave appears in the jet centerline which can also be observed in Case 1. But the distance between the reflection point, which beyond the computational domain, and the nozzle exit plane is much longer than the counterpart of Case 1. Besides, the angle formed by the oblique shock wave at the corner of the nozzle exit is also much larger. Again, as can be readily seen, there are good agreements between the experimental configurations of Ref. [1] and the computational results.

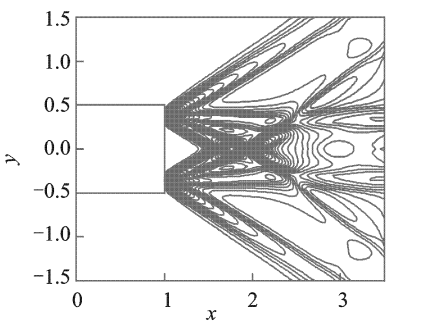

(a) Density contours

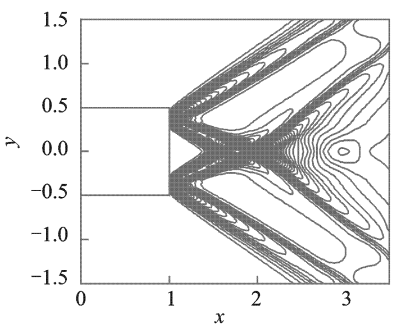

(b) Pressure contours

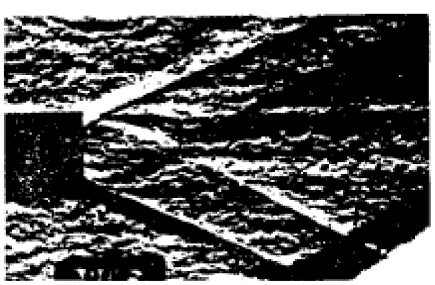

(c) Experimental shadowgraph[1]

Fig. 2 Contours for Case 1 and experimental shadowgraph

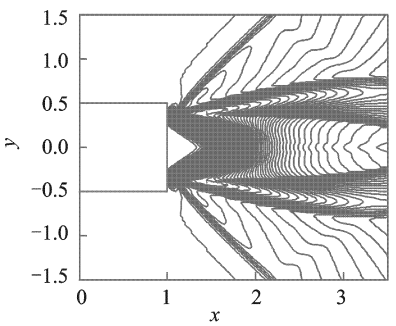

(a) Density contours

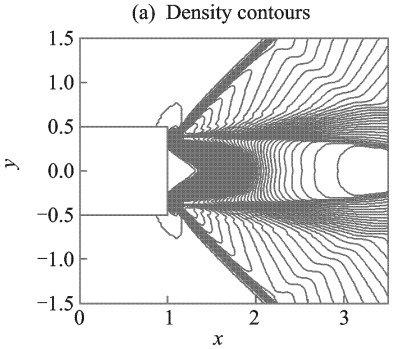

(b) Pressure contours

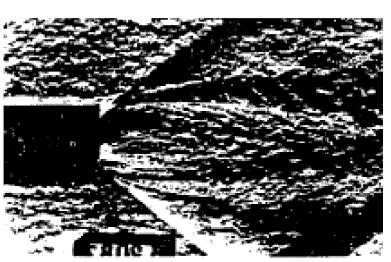

(c) Experimental shadowgraph[1]

Fig. 3 Contours for Case 2 and experimental shadowgraph

Fig. 4 shows the property contours of supersonic flow including the density, pressure and Mach number corresponding to Case 3. From these contours it can be seen that good resolution is also achieved. Comparised with the results of Case 2 show that when keeping the Mach number of supersonic freestream and the ratio of nozzle exit gas stagnation pressure to ambient gas static pressure invariant, as the temperature of the exhaust jet increasing, the angle caused by the oblique shock wave is almost without changing. But the distance between the reflection point and the nozzle exit plane become much smaller. These phenomenon can also be found in Ref. [5].

Fig. 5 shows the comparisons of the resulting distributions of the pressure along the nozzle wall corresponding to the Case 1 and Case 2, which are obtained by the positive schemes numerically and by Agrell and White[1] experimentally respectively, where p/p_∞ is the ratio of local gas pressure to ambient gas static pressure. Excellent agreements between the experimental measurements and the numerical solutions are found. In general, as shown in Fig. 5, the pressures of nozzle wall show almost no change except slightly decreasing near nozzle exit. In fact, as the supersonic external flow over the missile afterbody the jet shock is compressed by the supersonic freestream, the nozzle wall pressure almost equal to the ambient gas pressure.

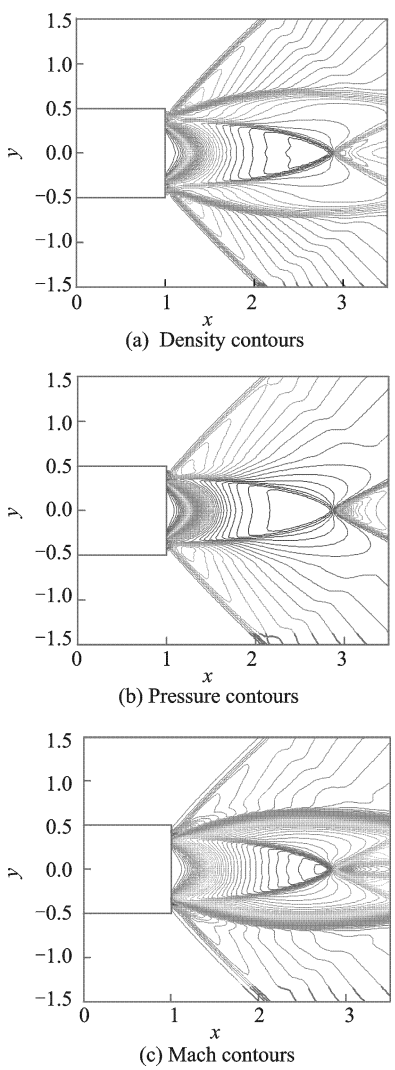

Fig. 4 Contours for Case 3

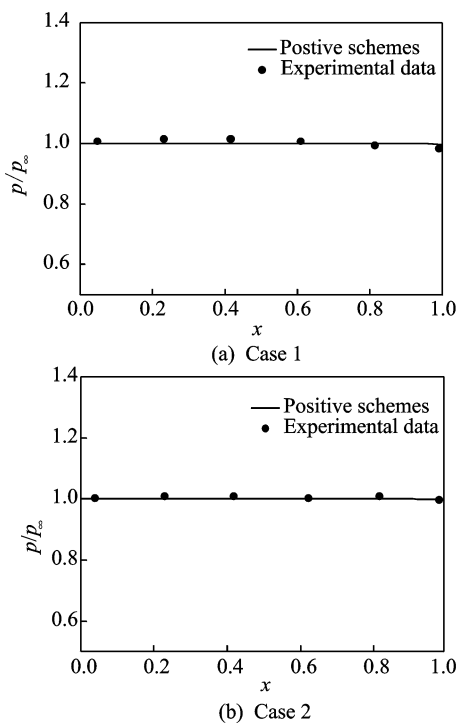

Fig. 5 Pressure distribution on nozzle wall

Fig. 6 shows the comparisons of centerline gas pressure distributions corresponding to Case 1, Case 2 and Case 3, which are obtained by TVD scheme with second order accuracy and RKDG finite element method with third order accuracy respectively, where p/p_j is the ratio of local gas pressure to jet exit gas stagnation pressure. The comparisons between the computed results obtained by presented method and those of Ref. [6] using the RKDG finite element method show good

agreement, which indicates positive schemes has high ability to capture shock waves. And the comparisons with numerical results of Ref. [5] using the TVD scheme show relatively good agreement, although same discrepancies exist. Those discrepancies are probably attributed to the difference of the ability to capture discontinuous points between the two methods. When the incident shock wave reflected on the jet centerline, the Mach number reduces and the pressure increases rapidly. As shown in Figs. 6(a,c), the computed results obtained by the positive schemes have much larger pressure gradient than those of TVD scheme, which indicates the presented method have much higher ability to capture the discontinuous points.

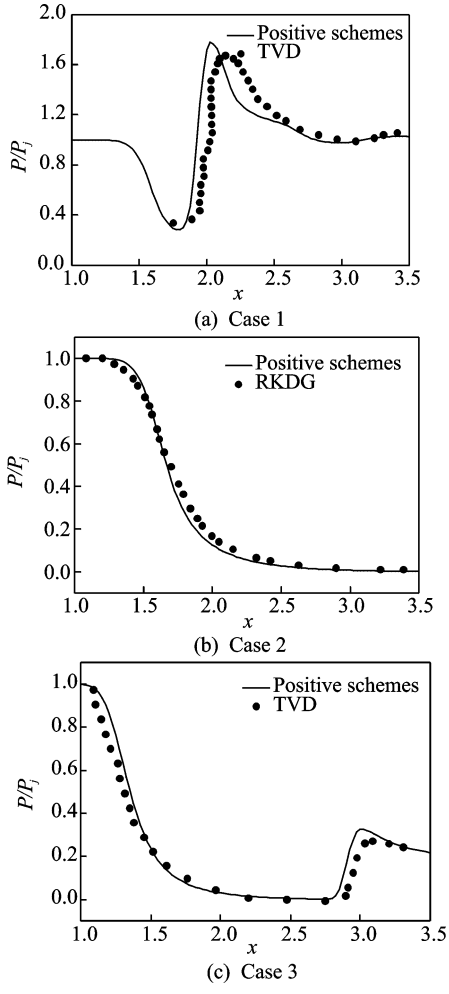

Fig. 6 Pressure distribution along jet axis

3 CONCLUSION

A detailed computational study is made for a *Ma* 2.01 external supersonic flow over a missile afterbody with supersonic centered propulsive jet exit *Ma* 2.5, using the developed second order accurate positive schemes method. Qualitative features of the extremely complex flow-field structures due to the interactions between the supersonic jet exhausting from the nozzle and the external supersonic flows, such as external compression shock, exhaust plume shape and trailing shock observed in experiments are successfully reproduced by the presented method. Also the influence of the supersonic afterbody jet flow fields is investigated by different pressure ratios and temperature ratios. Comparisons of computed results with experimental data and the existing numerical results obtained by RKDG finite element method and TVD scheme justify the proposed method used for the numerical simulation of such complex flow fields.

References:

[1] Agrell J, White R A. An experimental investigation of supersonic axisymmetric flow over boattails containing a centered propulsive jet [R]. FFA Technical Note, AU-913, 1974.

[2] Viswanath P R, Patil S R. Effectiveness of passive devices for axisymmetric base drag reduction at Mach 2 [J]. Journal of Spacecraft and Rockets, 1990, 27(3): 234-237.

[3] Petrie H L, Walker B J. Comparison of experiment and computation for a missile base region flow field with a centered propulsive jet [R]. AIAA-85-1618, 1985.

[4] Chapman D R. An analysis of base pressure at supersonic velocities and comparison with experiment [R]. NACA Report1051,1951.

[5] Le G G, Ma D W, Zang G C. Numerical simulation of flow in rocket base by TVD [J]. Journal of Ballistiscs, 1995, 7(1): 35-40. (in Chinese)

[6] Chen E Y, Ma D W, Le G G, et al. Discontinuous finite element method for supersonic flow of a missile propulsive jet [J]. Chinese Journal of Computational Physics, 2008, 25(6): 705-710. (in Chinese)

[7] Sahu J, Nietubitz C J. Numerical computation of base flow for a missile in the presence of a centered jet [R]. AIAA-84-0527, 1984.

[8] Sahu J. Computations of supersonic flow over a missile afterbody containing an exhaust jet [R]. AIAA-85-1815, 1985.

[9] Liu X D, Lax P D. Positive schemes for solving multi-dimensional hyperbolic systems of conservation laws [J]. CFD Journal, 1996, 5(2): 133-156.

[10] Liu X D, Lax P D. Positive schemes for solving multi-dimensional hyperbolic systems of conservation laws II [J]. Journal of Computational Physics, 2003, 187(2): 428-440.

[11] Chen E Y, Ma D W, Le G G, et al. Numerical simulation of highly underexpanded axisymmetric jet with Runge-Kutta discontinuous Galerkin finite element method [J]. Journal of Hydrodynamics, 2008, 20(5): 617-623.

[12] Sweby P K. High resolution schemes using flux limiters for hyperbolic conservation laws [J]. SIAM Journal on Numerical Analysis, 1984, 21(5): 995-1011.

[13] Kurganov A, Tadmor E. New high-resolution central schemes for nonlinear conservation laws and convection-diffusion equations [J]. Journal of Computational Physics, 2000, 160(1): 241-282.

[14] Shu C W. Total-variation-diminishing time discretizations [J]. SIAM Journal on Scientific and Statistical Computing, 1988, 9(6): 1073-1084.

[15] Shu C W, Osher S. Efficient implementation of essentially non-oscillatory shock-capturing schemes, II [J]. Journal of Computational Physics, 1989, 83(1): 32-78.

弹尾超声速轴对称喷流的正格式数值模拟

朱孙科[1] 马大为[1] 陈二云[2] 乐贵高[1]

(1. 南京理工大学机械工程学院,南京, 210094, 中国;2. 上海理工大学能源与动力学院,上海, 200093,中国)

摘要:采用二阶正格式方法对超声速轴对称喷流流动进行数值模拟。将二维守恒方程的正格式方法发展到轴对称Euler方程组的求解,并对导弹尾部超声速伴随射流进行了数值计算。数值结果与实验照片所反映的流动特征吻合较好,与三阶精度间断有限元方法计算结果吻合,相比于二阶高分辨率TVD格式的计算结果,正格式方法的计算结果在间断点处具有较大的梯度变化。这表明该方法对激波具有较强的捕捉能力,在间断处不会出现数值振荡,对弹尾声音速伴随射流的数值模拟真实、有效。

关键词:计算流体力学; 超声速流动; 正格式; 数值模拟

中图分类号:V211.3

(Executive editor: Sun Jing)

基金项目:国防基础科研基金(A2620061288)资助项目; 上海市教育委员会重点学科(J50501)资助项目。